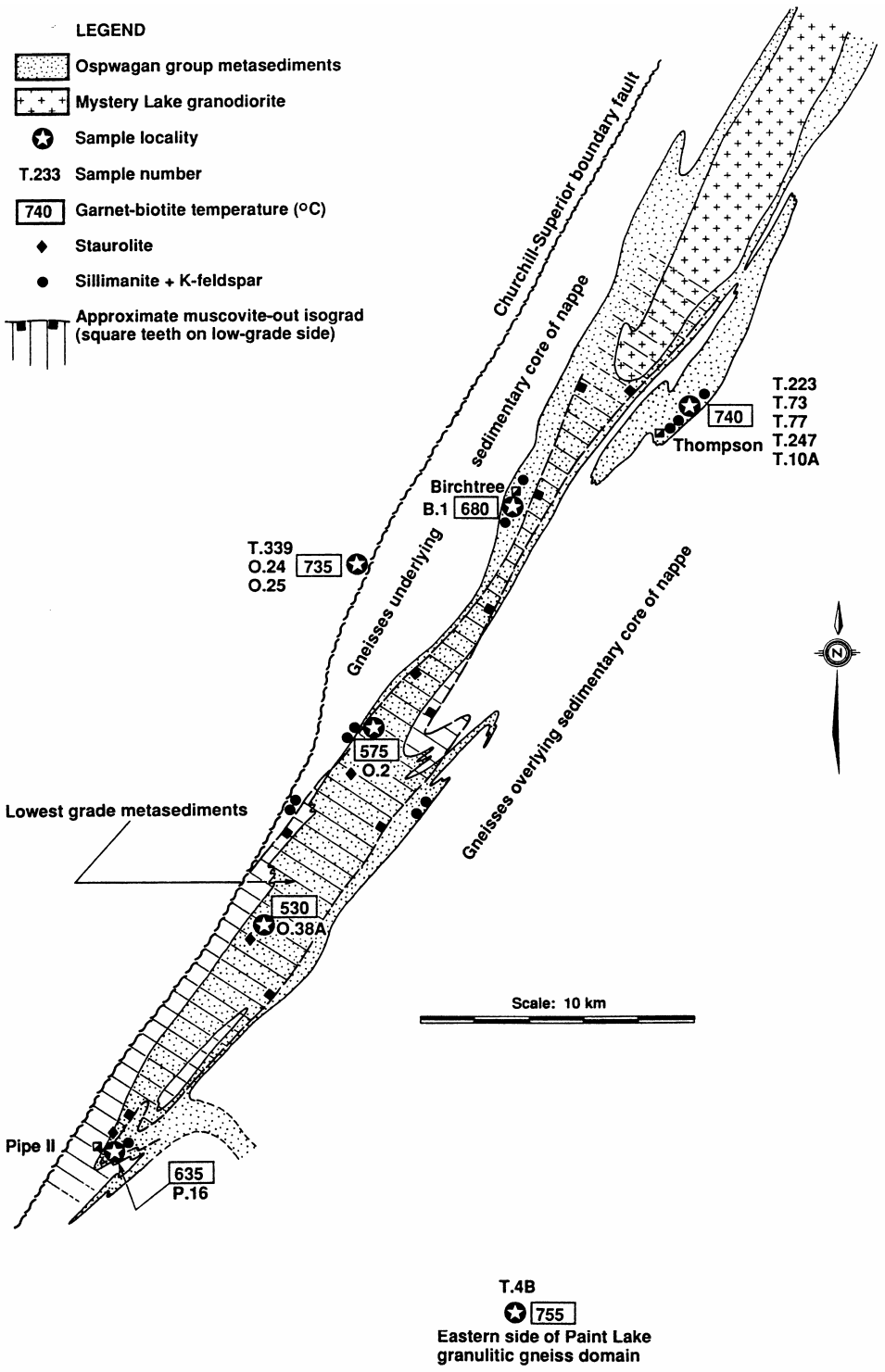

Figure 7.1 Metamorphic map of the Thompson – Pipe area of the TNB. Map identifies samples taken by Bleeker (1990), where boxes indicate average garnet – biotite temperatures attained using the Ferry and Spear calibrations (from Bleeker, 1990).

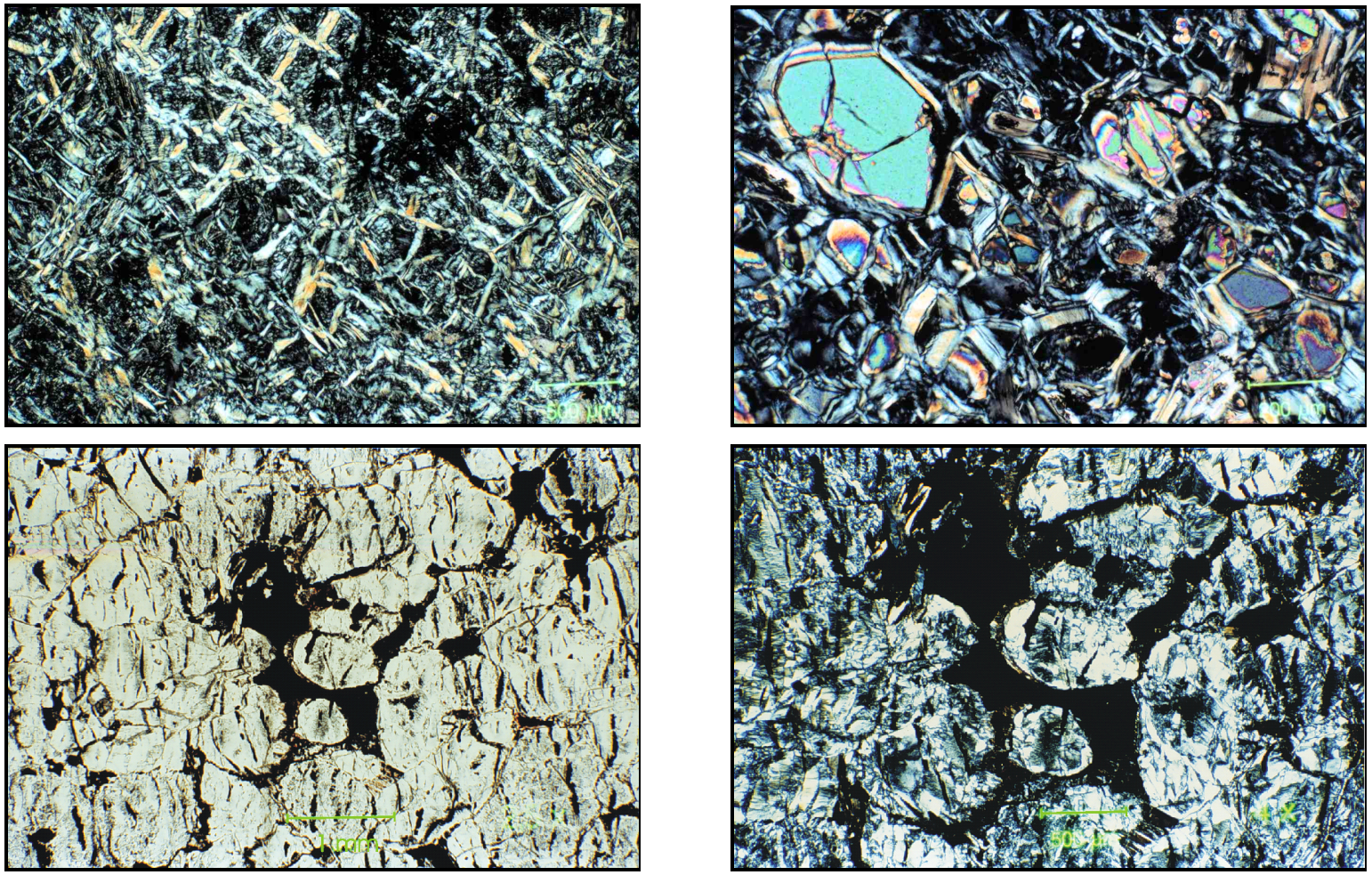

Figure 7.2 A) Top left, non-pseudomorphic recrystallization of serpentinized dunite in the W56 ultramafic body. Loss of α-lizardite at the expense of interpenetrating needles and blades of antigorite (DDH WL97-169, XPL, 500 µm scale bar). B) Top right, non-pseudomorphic recrystallized serpentine in partially serpentinized dunite, with relict fragments of olivine (DDH WL96-179, XPL, 200 µm scale bar). C) Lower left, transitional-textured complete serpentinization of dunite in the Pipe 1 ultramafic body showing magnetite produced during serpentinization preserving mesh textures, whereas interstitial magnetite preserving olivine ovoid morphologies (DDH 86232-3918, PPL, 1 mm scale bar). D) Lower right, same as C, but XPL (500 µm scale bar). Note the complete recrystallization of serpentine.

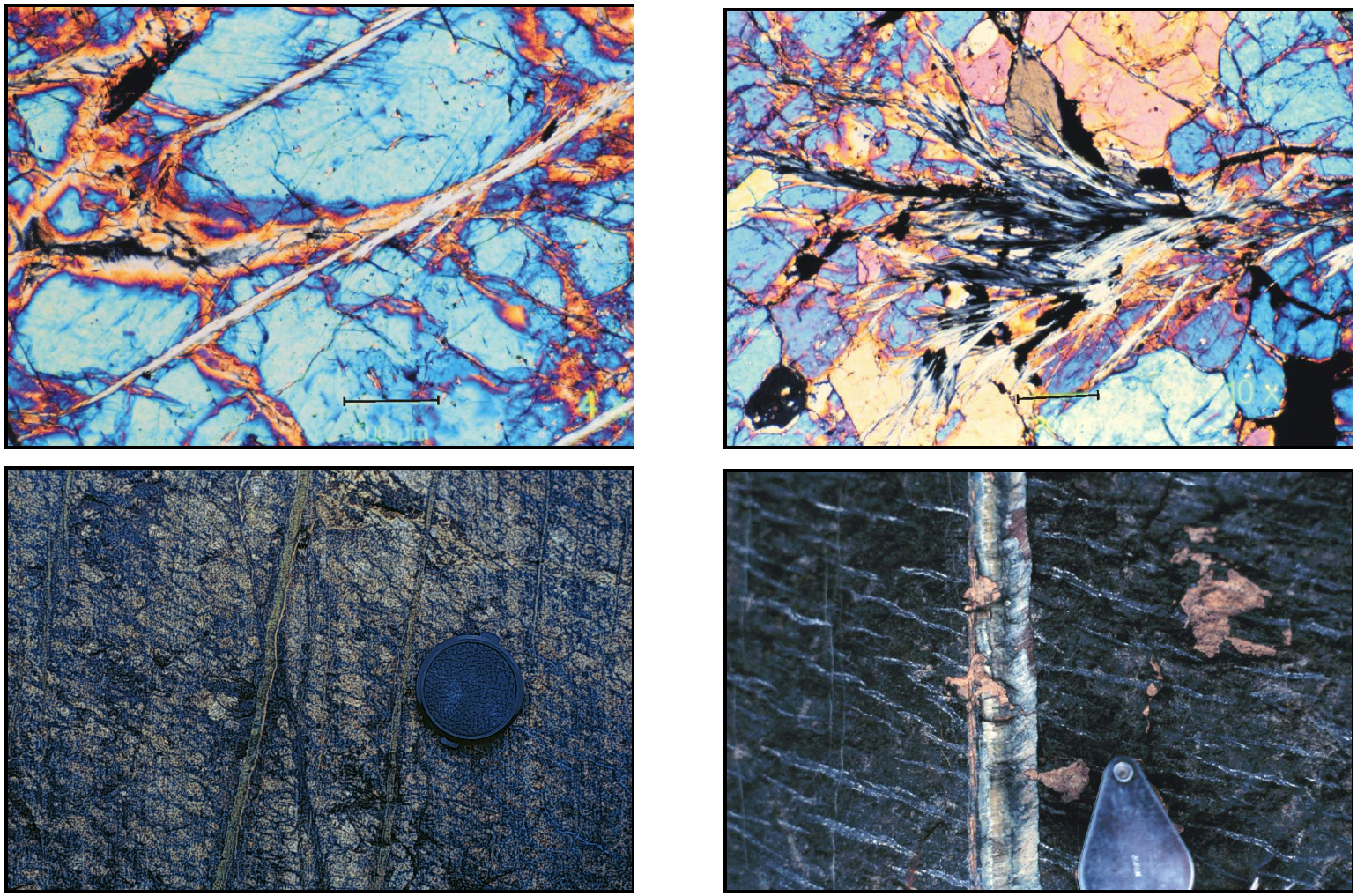

Figure 7.3 A) Top left, partially serpentinized dunite in the Brostrom ultramafic body showing non-penetrative partial serpentinization with late veinlet-oriented antigorite (DDH 89239-2119, XPL, 500 μm scale bar). B) Top right, late branching antigorite in the Brostrom Lake ultramafic body (DDH 89239-2119, XPL, 200 μm scale bar). C) Lower left, rare outcrop of ultramafic rocks (harzburgite described by Peredery, 1982) at the western margin of Pipe Pit. Veining crosscutting all primary and secondary fabrics, including magnetite veins produced during early serpentinization (lens cap ~5.5 cm). D) Lower right, close-up of C, note the crosscutting nature of the clinochrysotile vein (hand lens 2.5 cm wide).

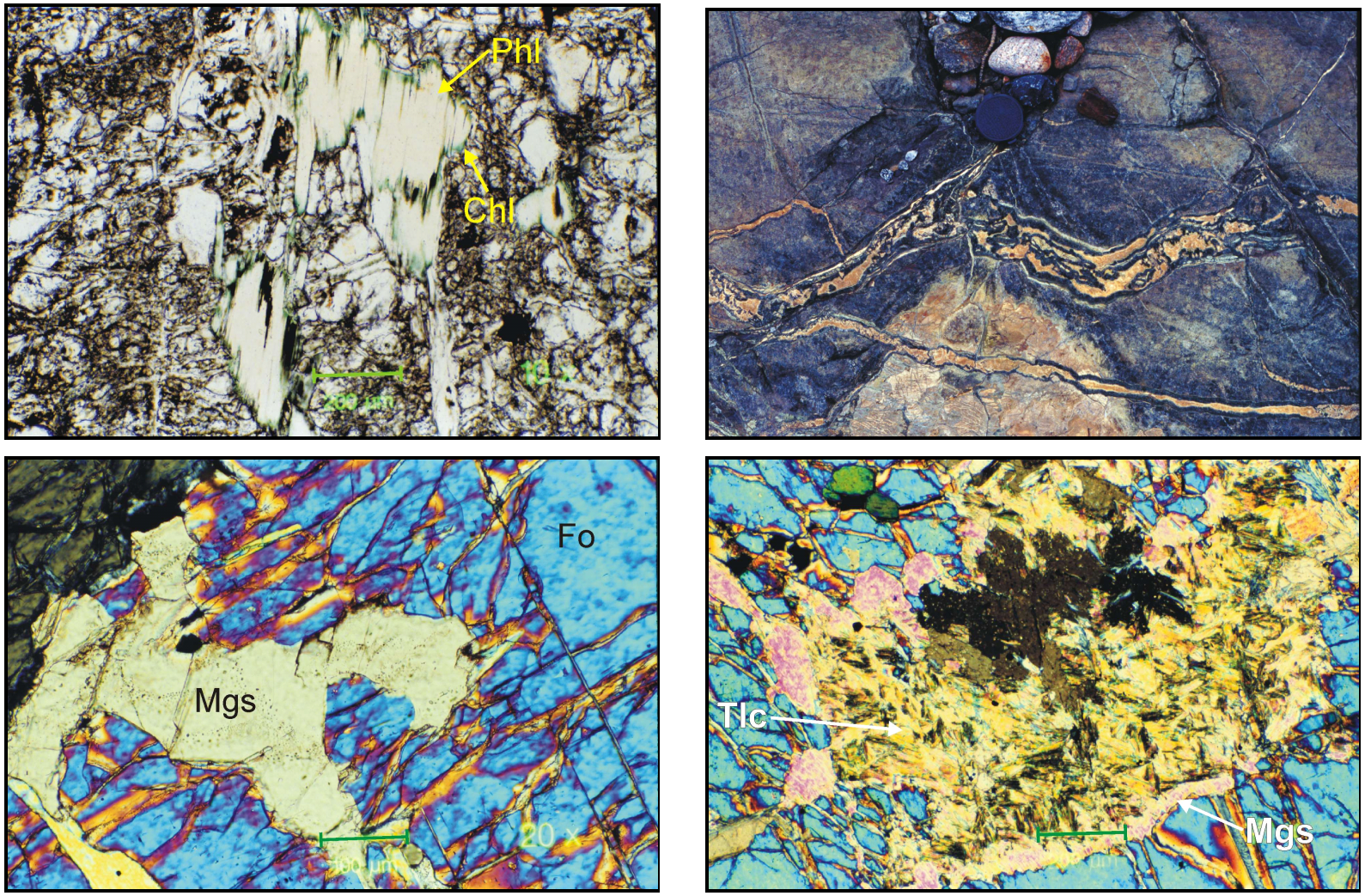

Figure 7.4 A) Top left, phlogopite rimmed with chlorite in a partially serpentinized dunite from the Brostrom Lake ultramafic body (DDH 89239-1991, PPL, 200 µm scale bar). B) Top right, crosscutting magnesite veining from the west margin of Pipe Pit (5.5 cm lens cap for scale). C) Lower left, late magnesite crosscutting olivine and α-lizardite (DDH 89239-2119, PPL, 100 µm scale bar). D) Lower right, late magnesite grain with core of 'feathery' talc that crosscuts all primary and secondary fabrics (DDH 89239-2119, PPL, 200 µm scale bar).

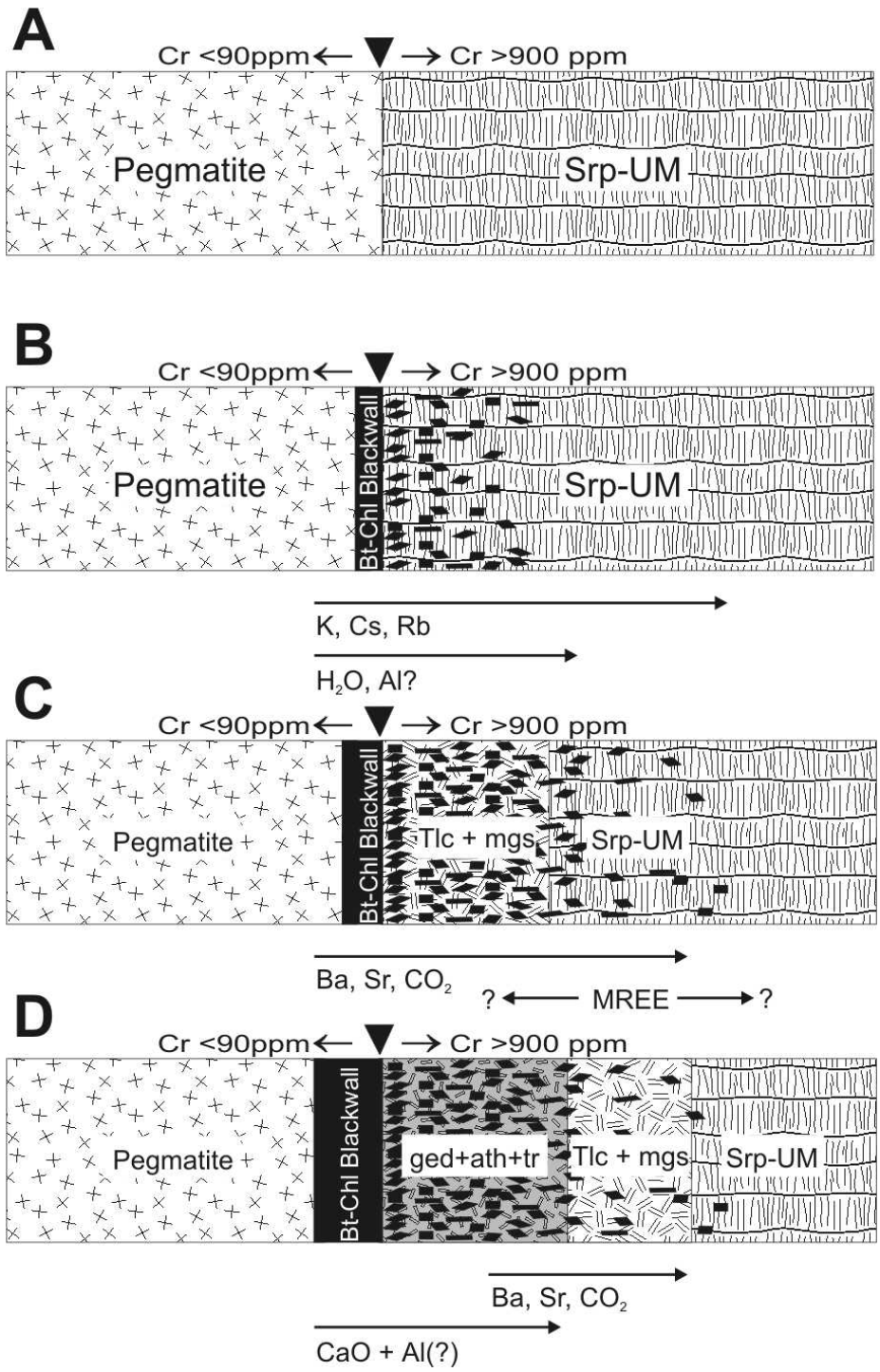

Figure 7.5 Schematic diagrams (not to scale) showing the mobility of elements during the production of alteration zones in ultramafic rocks adjacent to granitic pegmatites. Figures A-D are an interpreted timeline in the production of alteration zones. The pegmatite-ultramafic contact was inferred from the contrast in Cr contents. A) Initial pegmatite injection. B) Development of a biotite-chlorite blackwall, with biotite porphyroblast growth in the serpentinized ultramafic rock. C) Continued development of a biotite-chlorite blackwall, and volatile metasomatism controlled by CO_2 diffusion with talc-carbonate growth D) Overgrowth textures indicate amphibole growth near the pegmatite contact controlled by Si and Al diffusion.

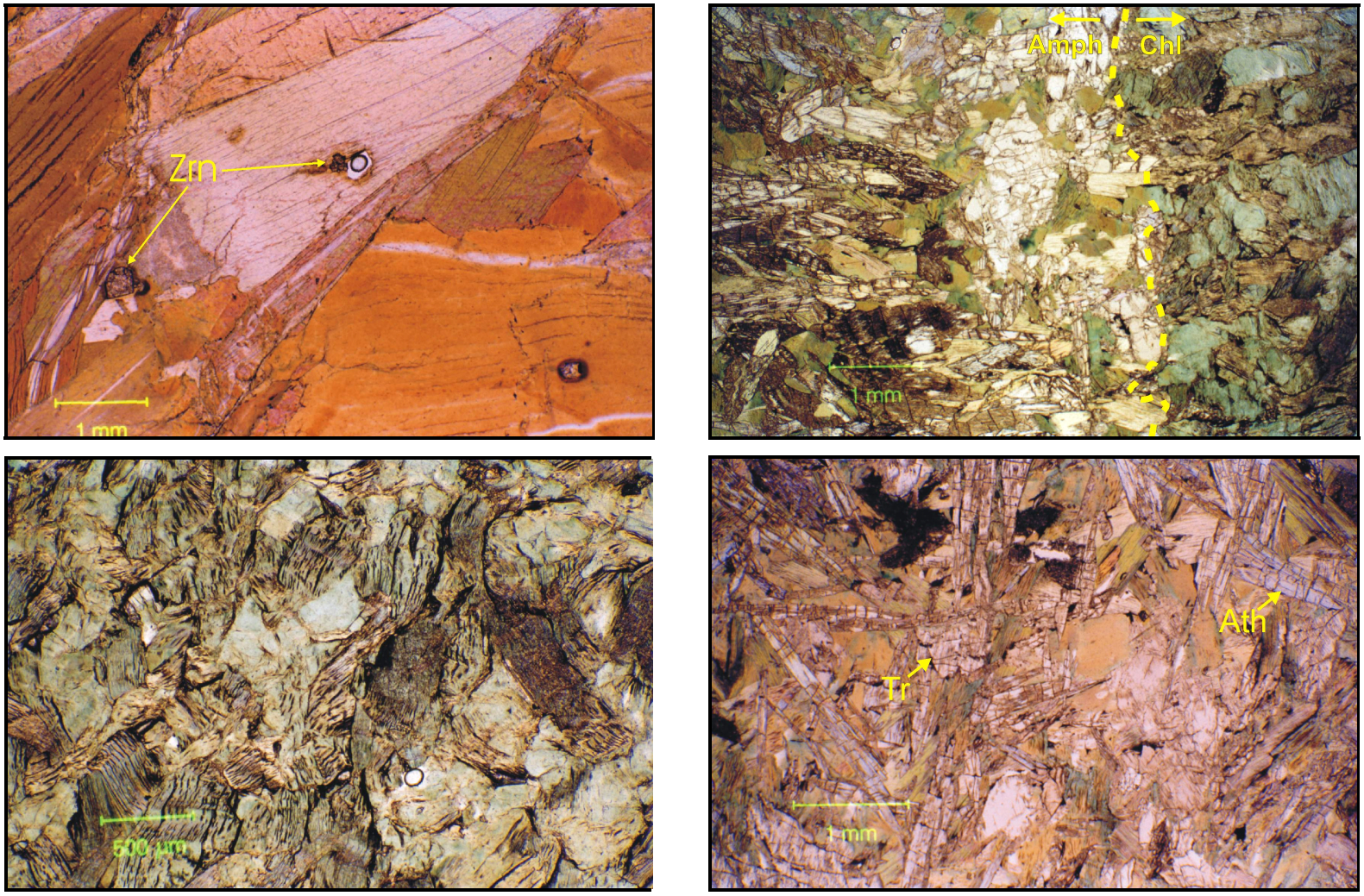

Figure 7.6 Photomicrographs of alteration zones. A) Top left, metamict zircon in biotite blackwall (DDH 86288-1982, PPL, 1 mm scale bar). B) Top right, chlorite blackwall (DDH WL96166-550E, PPL, 500 mm scale bar) C) Lower left, chlorite blackwall contact with amphibole zone dominated by gedrite + anthophyllite (DDH WL96166-550E, PPL, 1 mm scale bar). D) Lower right, amphibole zone close to talc-carbonate zone. Amphibole assemblage is anthophyllite-tremolite (WL96166-550D, PPL, 1 mm scale bar).

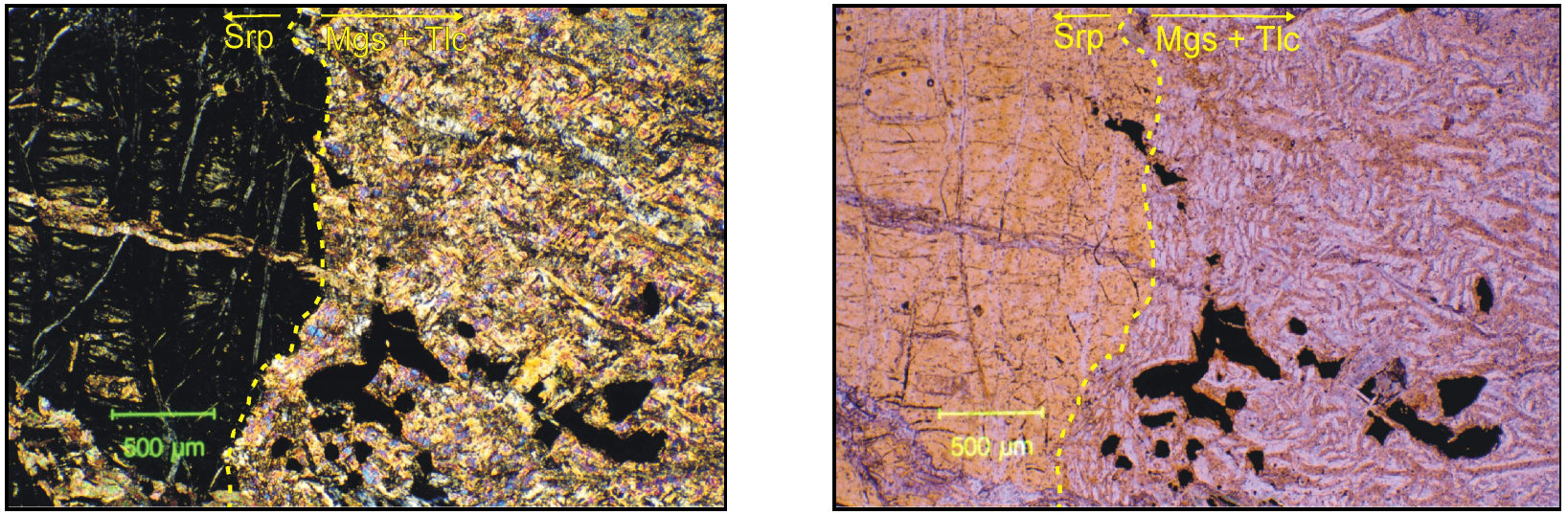

Figure 7.6 (contd.) Photomicrographs of alteration zones. E) Left, sharp ultramafic – talc-carbonate contact, showing coarse vermicular-textured talc-carbonate (Wl96166-550B, PPL, 500mm scale bar). F) Right, same as E), but XPL.

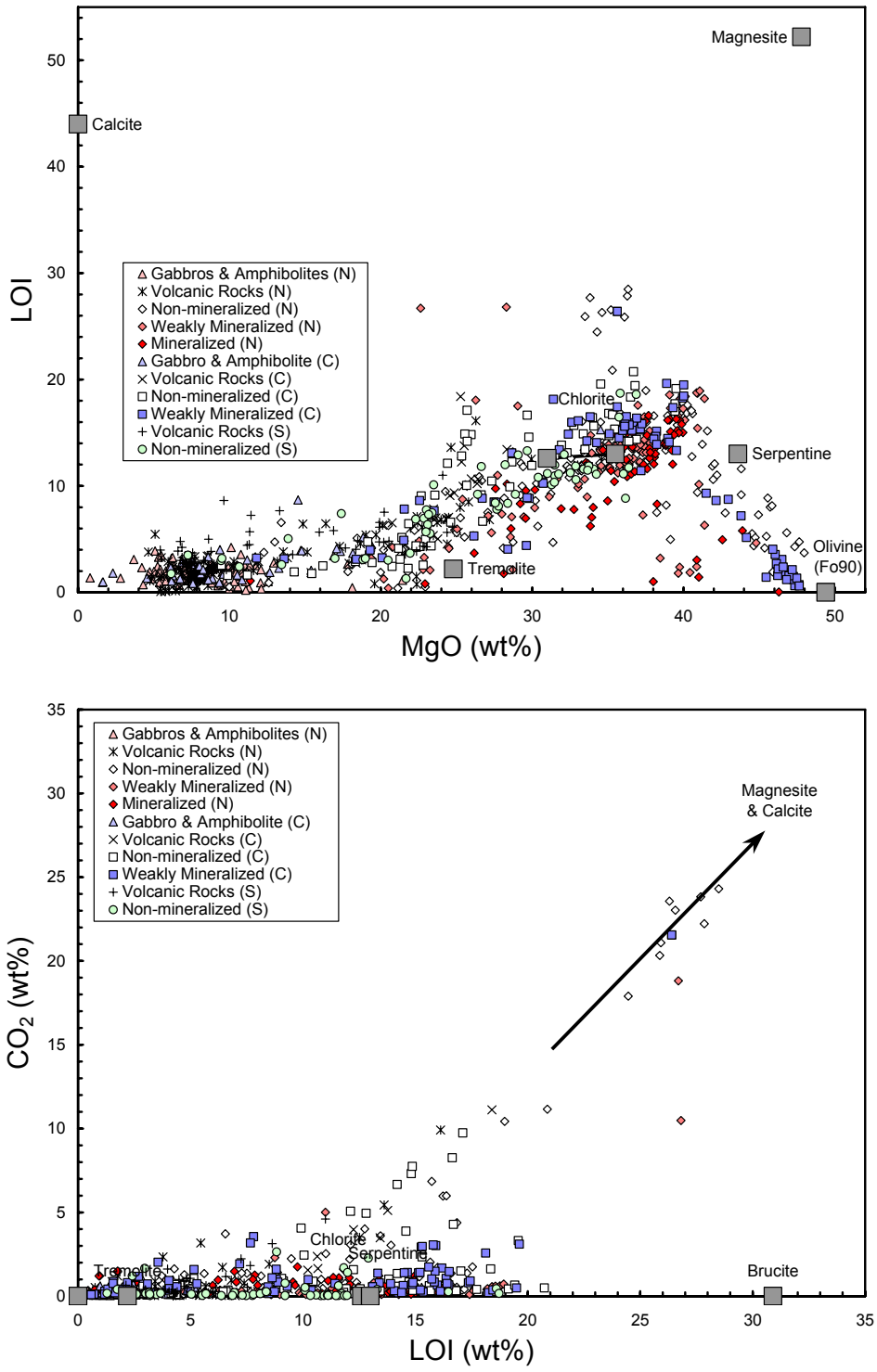

Figure 7.7 A) Variation in LOI as a function of MgO content (not volatile corrected) for mafic and ultramafic rocks from the TNB. There is a general trend of increasing LOI with increasing MgO, indicating that peridotitic and dunitic lithologies are more susceptible to serpentinization owing to the greater abundances of olivine. B) CO_2 vs. LOI indicating that the samples containing LOI contents in excess of that which can be accommodated in serpentine is normally attributable to the presence of carbonate minerals. Samples with high LOI and low CO_2 are attributable to brucite (O'Hanley, 1996).

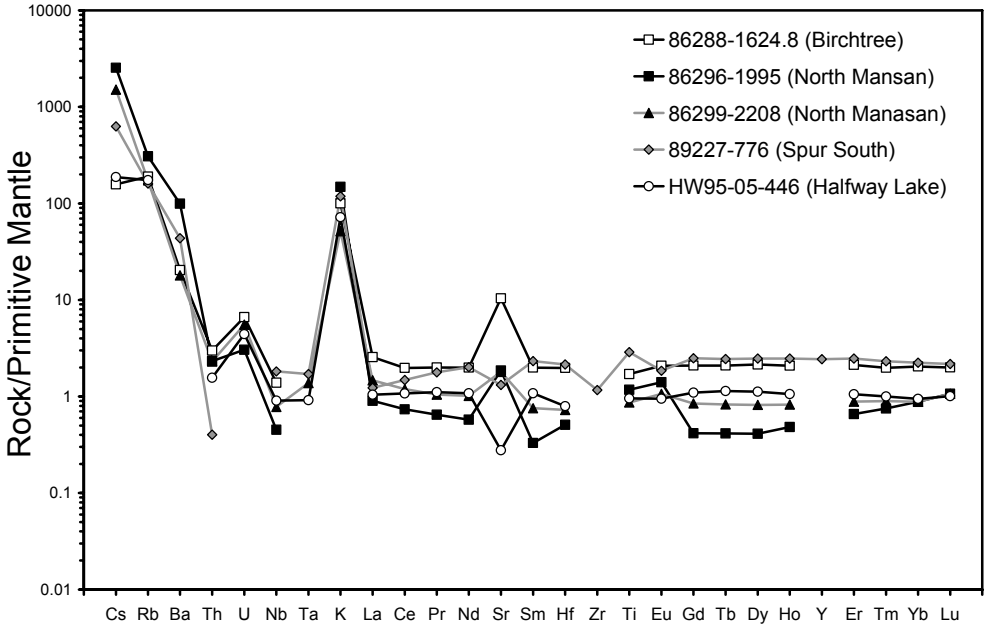

Figure 7.8 Mantle-normalized multi-element plot showing enrichment in Cs > Rb > K > Ba (> Sr) > U accompanying K metasomatism. Mantle normalization values from McDonough and Sun (1995).

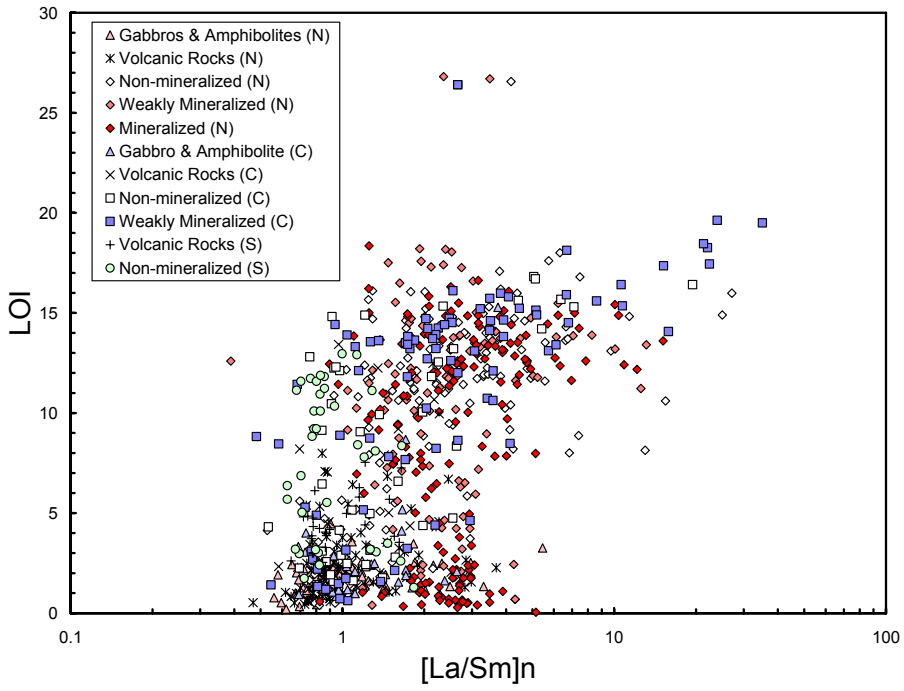

Figure 7.9 Plot of $[La/Sm]_n$ vs. total LOI for serpentinized TNB ultramafic bodies. There is a general trend of increasing $[La/Sm]_n$ with increasing LOI within individual ultramafic bodies, suggesting a correlation between LREE enrichment and metasomatism (e.g., William Lake, blue squares). Abbreviations: N, northern region of the TNB; C, central region of the TNB; S, southern region of the TNB. Mantle normalization values from McDonough and Sun (1995).

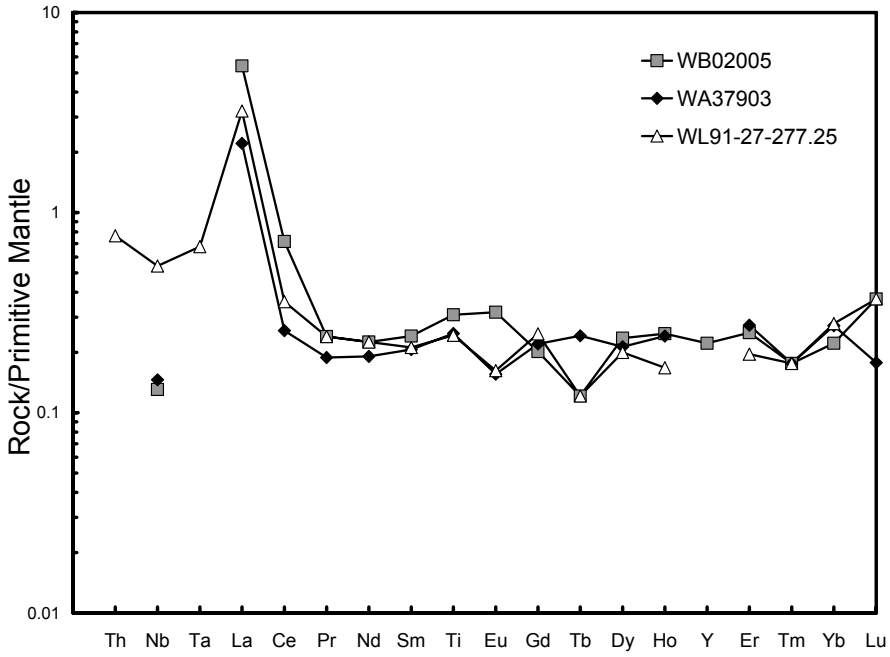

Figure 7.10 Primitive mantle normalized REE plot, showing the high La/Ce ratios of some samples from the TNB. Mantle normalization values from McDonough and Sun (1995).

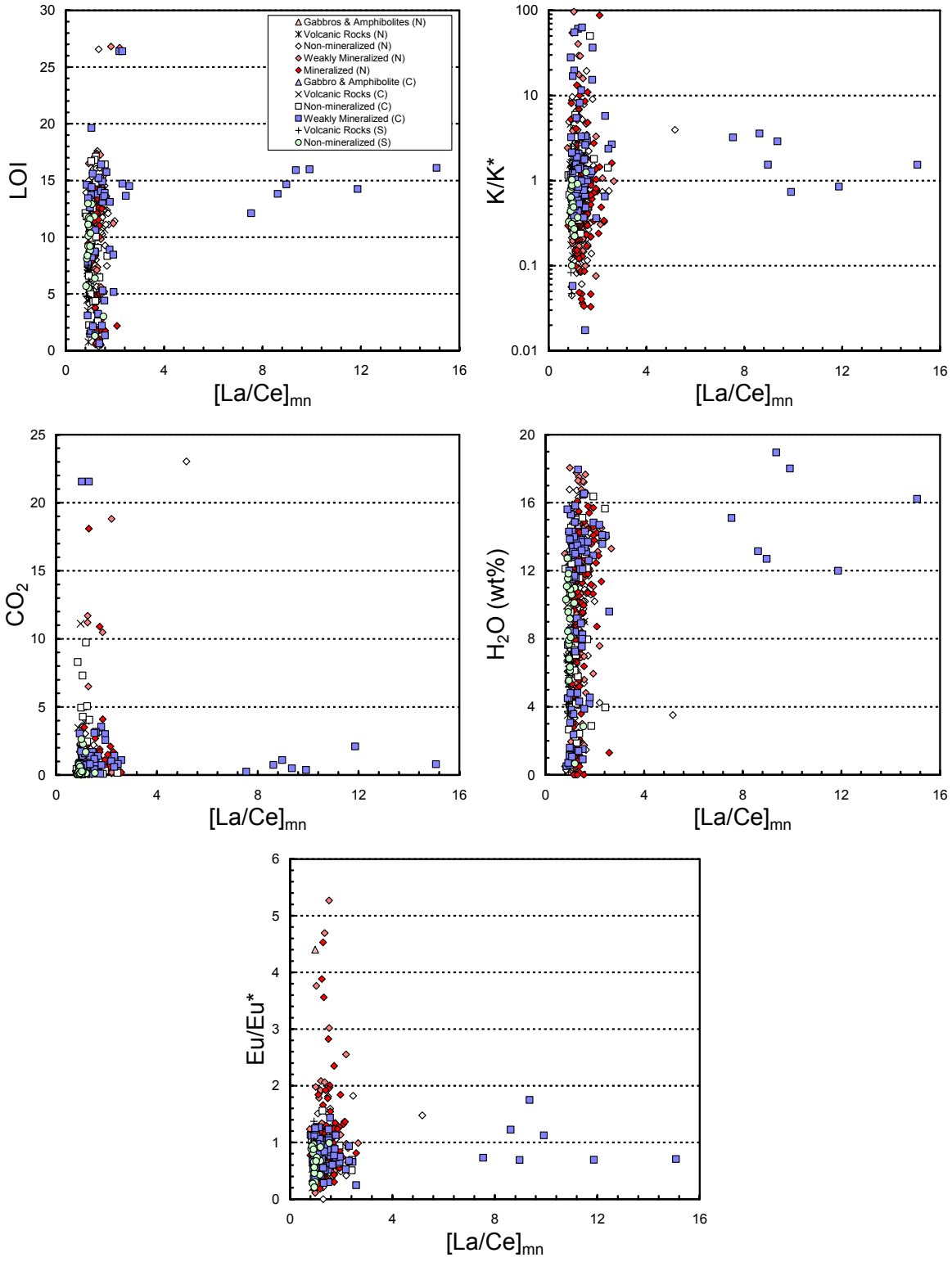

Figure 7.11 Mantle-normalized La/Ce ratios as a function of LOI, K/K*, CO_2, Eu/Eu* and H_2O for 190 ultramafic rocks from the central TNB. All samples contain abundances significantly above detection limits. Mantle normalization values from McDonough and Sun (1995).

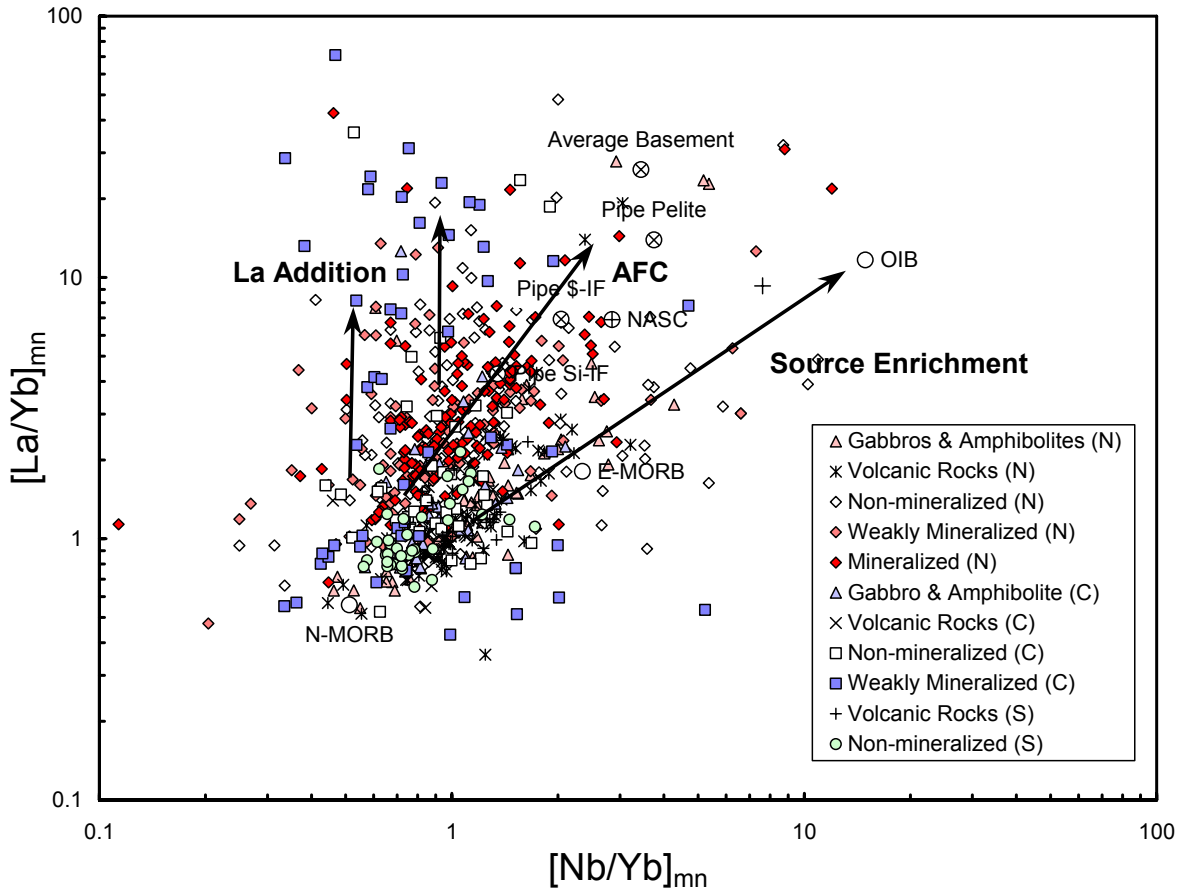

Figure 7.12 Plot of $[La/Yb]_{mn}$ vs. $[Nb/Yb]_{mn}$ for TNB ultramafic rocks. All values are significantly above detection limits (0.1 ppm La, 0.05 ppb Nb and Yb). Mantle normalization values from McDonough and Sun (1995). Reference compositions: N-MORB, Normal MORB, Sun and McDonough (1989); E-MORB, enriched MORB, trace elements from Sun and McDonough (1989); OIB, Ocean Island Basalt, trace elements from Taylor and McLennan (1985); NASC, North American Shale Composite, Gromet et al. (1984); Pipe $-IF, lowermost sulfide facies iron formation from Pipe Pit (CHA-35); Pipe $-IF, P_3 silicate facies iron formation from Pipe Pit (CHA125); Pipe Pelite (CHA33); Average Basement, average of 18 basement rocks collected during this project.

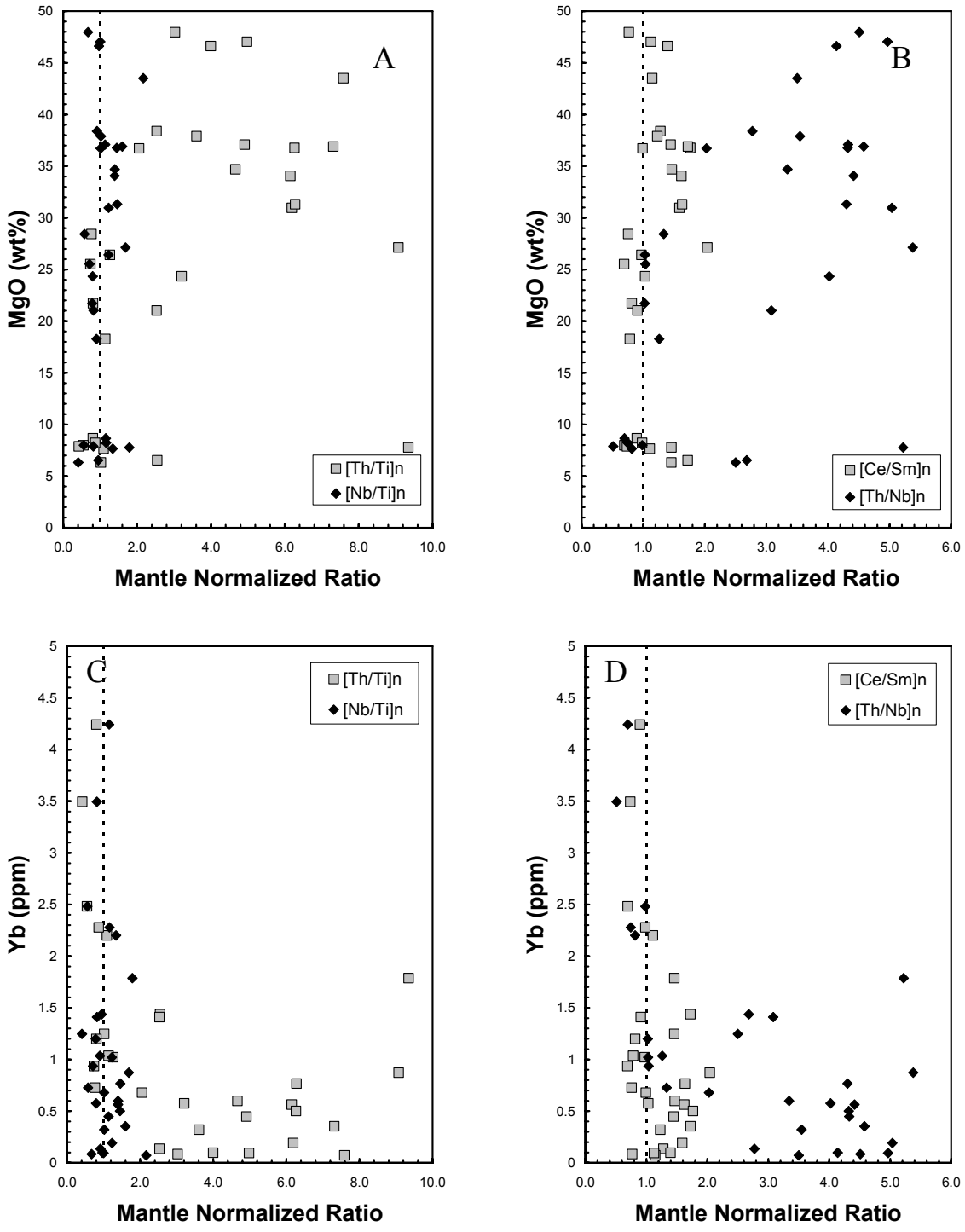

Figure 7.13 Plots of trace element enrichment as a function of Yb and MgO content in the Mystery Lake ultramafic body (DDH 89225, 89234 and 89236). Mantle normalization values from McDonough & Sun (1995).

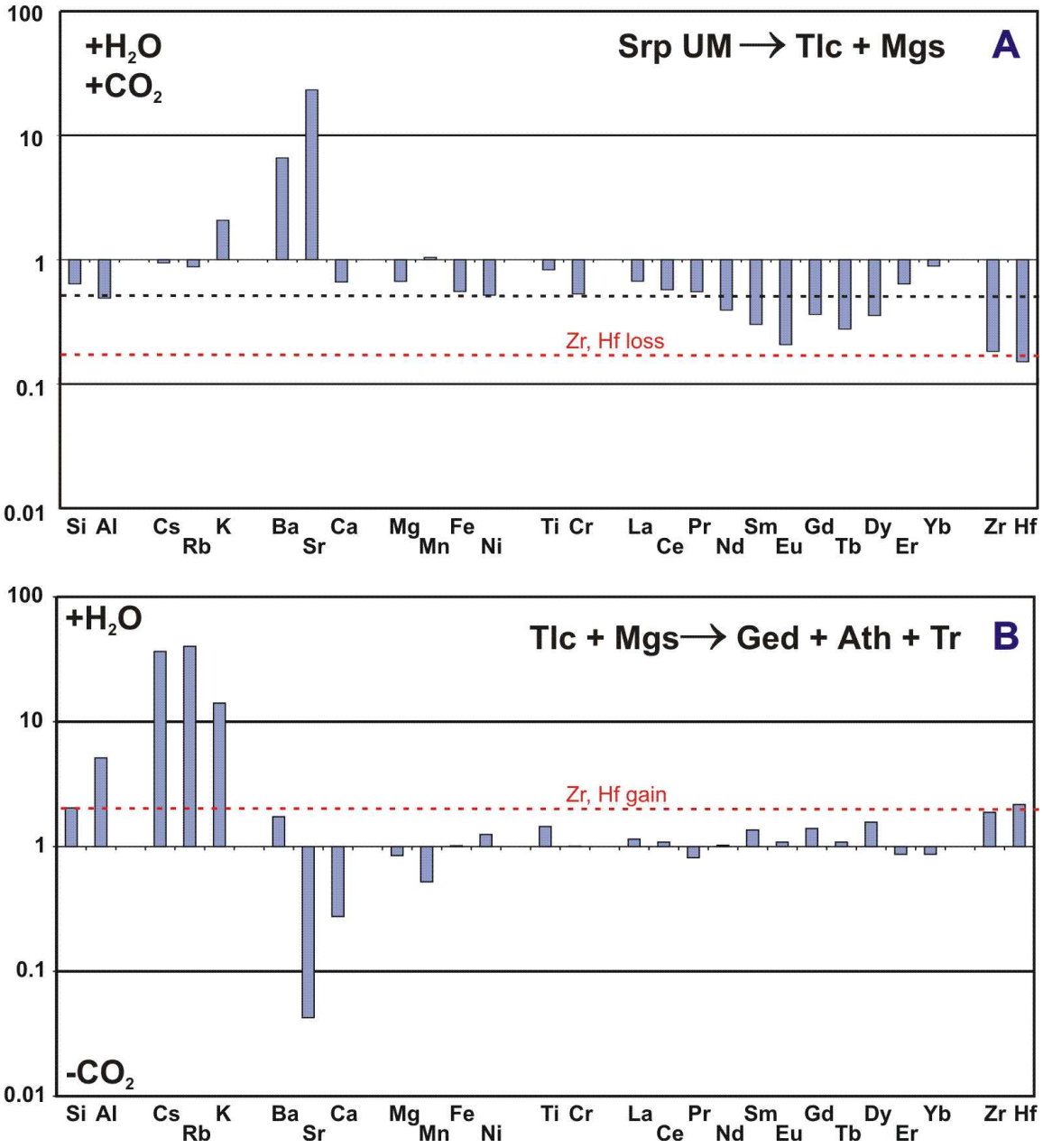

Figure 7.14 Enrichment - depletion diagrams showing composition of talc-magnesite zone relative to serpentinized ultramafic zone (A) and amphibole zone relative to talc-magnesite zone (B). Calculations were based on the method of Gresens (1967) with correction for density. Elements are grouped by charge and ordered according to decreasing ionic radius. Dashed line indicates zero mass change assuming Cr was immobile (see **Section 7.2.3.2** for discussion). Note that Zr and Hf were mobilized from talc-magnesite zone to amphibole zone, consistent with petrographic evidence for metasomatic zircon and that REE were fractionated during talc-carbonation but not amphibolitization.

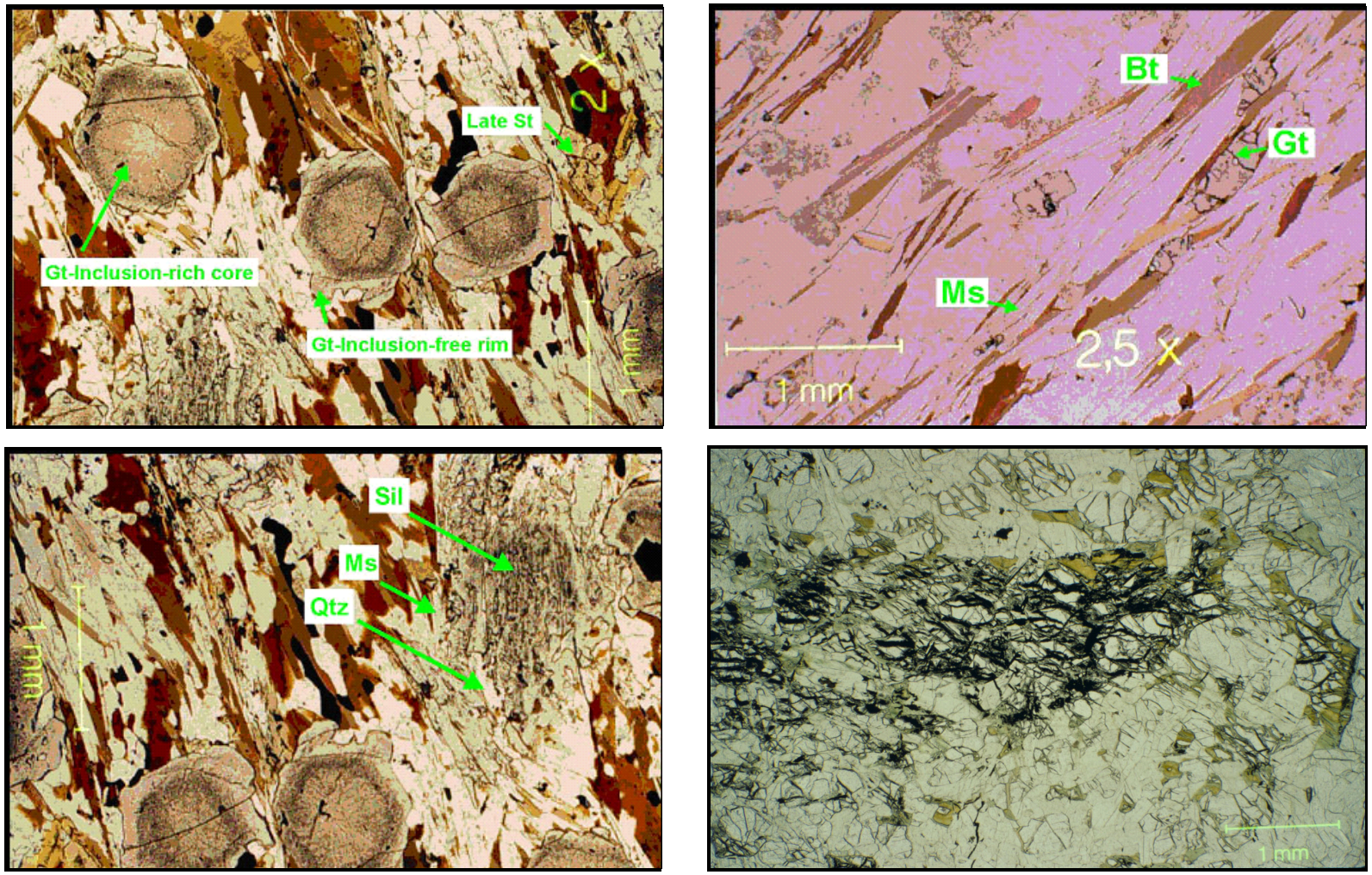

Figure 7.15 Photomicrographs of metapelites and metabasalts used in P-T estimates for the central TNB. A) Top left, first style (Gt1) of garnet porphyroblasts with two stages of growth. Cores record original euhedral shape, whereas late overgrowths are anhedral. Overgrowth garnet appears to be temporally equivalent to the late staurolite also seen in this photomicrograph (WB09867, PPL, 1mm scale bar). B) Top right, second style (Gt2) of garnet that forms anhedral grains parallel to the foliation (WB09853, PPL, 1mm scale bar). C) Lower left, relict prograde sillimanite partially altered to retrograde muscovite and quartz (WB09867, PPL, 1mm scale bar). D) Lower right, olivine porphyroblast associated with dark green to brown-green spinel and orthopyroxene (WB02077, 1mm scale bar).

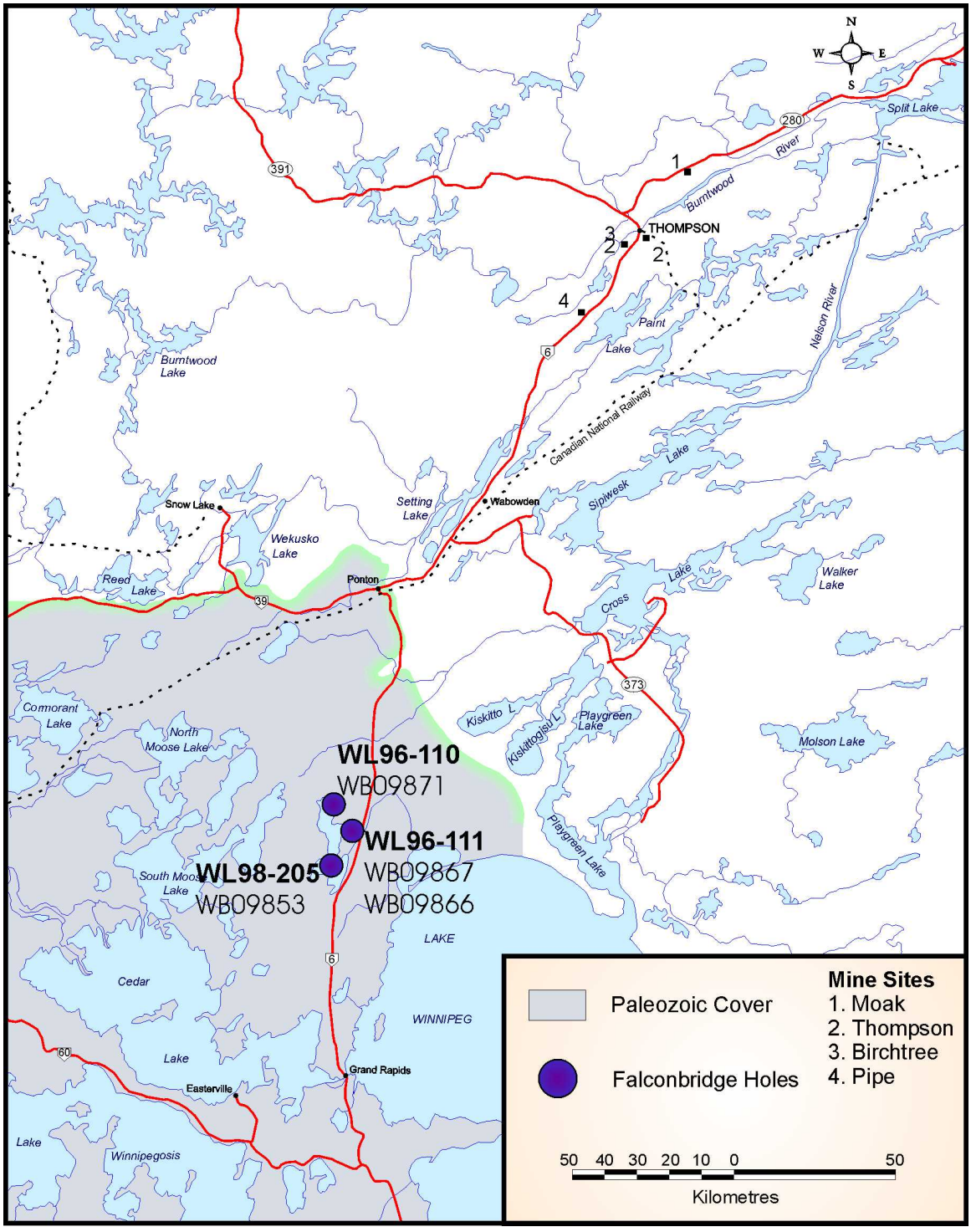

Figure 7.16 Location of the drillholes and samples used in geothermometry and geobarometry.

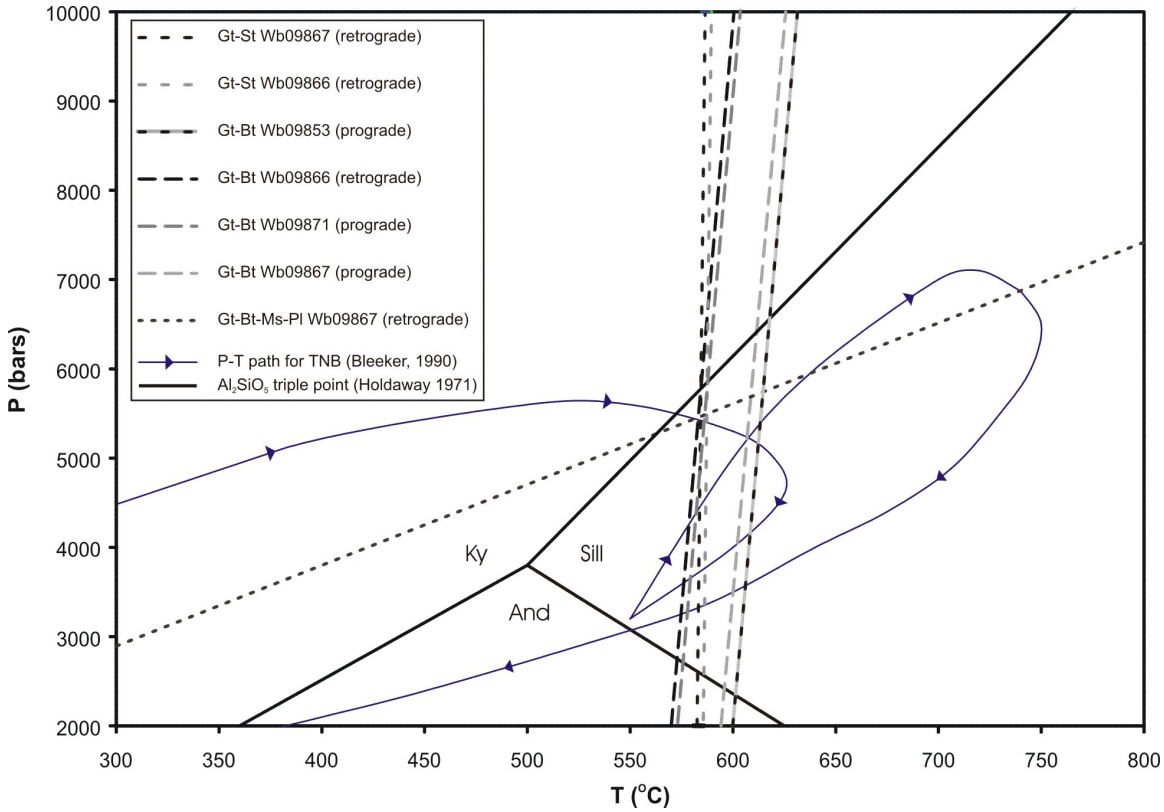

Figure 7.17 Summary of geothermometric and geobarometric data obtained for metasedimentary rocks during this study. Garnet (core) and biotite (inclusions and matrix) equilibria suggest minimum peak temperatures of ~600±50°C and retrograde temperatures of ~575±50°C for garnet overgrowths. Garnet-staurolite-sillimanite equilibria suggest ~575±50°C for retrograde garnet+staurolite growth (at fH_2O = 0.1-0.3). One sample (WB09867) allowed geobarometry, yielding 3-7 kbar and an intersection with retrograde garnet overgrowths at 5.5 kbar and ~575°C.